processes

MDPI

*Article*

# Optimization of Milling Process Parameters for Waste Plum Stones for Their Sustainable Application

**Nataša Gajić [1,*], Dragana Radovanović [1], Jovana Đokić [2], Ivana Jelić [3], Sanja Jevtić [4], Katarina Sokić [4] and Marija Štulović [1]**

[1] Innovation Center of the Faculty of Technology and Metallurgy, Belgrade Ltd., University of Belgrade, Karnegijeva 4, 11000 Belgrade, Serbia; divsic@tmf.bg.ac.rs (D.R.); mstulovic@tmf.bg.ac.rs (M.Š.)
[2] Innovation Centre of the Faculty of Chemistry in Belgrade Ltd., University of Belgrade, Studentski Trg 12-16, 11000 Belgrade, Serbia; djokic@chem.bg.ac.rs
[3] Institute for Technology of Nuclear and other Mineral Raw Materials, Franchet d'Esperey 86, 11000 Belgrade, Serbia; i.jelic@itnms.ac.rs
[4] Faculty of Technology and Metallurgy, University of Belgrade, Karnegijeva 4, 11000 Belgrade, Serbia; sanja@tmf.bg.ac.rs (S.J.); ksokic@tmf.bg.ac.rs (K.S.)
* Correspondence: ngajic@tmf.bg.ac.rs; Tel.:+381-605236021

## Abstract

The impact of milling process parameters on the physicochemical properties of waste plum stones was investigated to enable their further utilization as a functional material. The experiments were conducted using a planetary ball mill, with variations in milling duration (1–3 h), the ball-to-powder ratio (bpr) (10:1 and 20:1), and the rotation speed (250 and 500 rpm). Transformations of material in a function of process parameters were assessed by XRD, FTIR, and SEM analysis, revealing differences in particle size distribution, functional group composition, and surface morphology. Optimization of milling process parameters was focused on promoting fine particle formation and surface activation without causing significant material degradation. The best result was achieved with the PS-M10 sample, processed at a speed of 500 rpm and a bpr of 20:1 during a short milling time of 1 h. The milled sample demonstrated promising potential for further applications, particularly for heavy metal ion ($Pb^{2+}$ and $Cu^{2+}$) removal from aqueous solutions through adsorption.

**Keywords:** biomass; planetary milling; physicochemical properties; $Pb^{2+}$ adsorption; $Cu^{2+}$ adsorption

check for updates

Academic Editor: Marcus Vinicius Tres

Received: 15 July 2025
Revised: 10 August 2025
Accepted: 20 August 2025
Published: 28 August 2025

**Citation:** Gajić, N.; Radovanović, D.; Đokić, J.; Jelić, I.; Jevtić, S.; Sokić, K.; Štulović, M. Optimization of Milling Process Parameters for Waste Plum Stones for Their Sustainable Application. *Processes* **2025**, *13*, 2759. https://doi.org/10.3390/pr13092759

**Copyright:** © 2025 by the authors. Licensee MDPI, Basel, Switzerland. This article is an open access article distributed under the terms and conditions of the Creative Commons Attribution (CC BY) license (https://creativecommons.org/licenses/by/4.0/).

## 1. Introduction

In the last several years, global production of plums has exceeded 12 million tons per year. Serbia ranks fourth among the world's plum producers, after China, Romania, and Chile, with a contribution of approximately 362.71 thousand tons, accounting for 2.9% of the world's production in 2023 [1]. A characteristic of the plum production sector in Serbia is highly structured domestic processing. Around 70% of the annual yield is used by the national agroindustrial complex [2]. In addition, plum processing leads to the generation of a significant amount of by-products such as plum stones with high potential value for sustainable use. Plum stones, containing approximately 61.1% carbon and composed mainly of cellulose, hemicellulose, and lignin, are considered a promising lignocellulosic biomass for many applications due to their favorable structure and chemical properties [3].

Recently, various plant wastes such as plum, fig, pea, and java plum seeds have been investigated as sources of energy, biosorbents, and materials for environmental protection [4–8]. The importance of such biomass-based materials has been increasingly

recognized in the context of circular-economy strategies. Giordano et al. identified biomass valorization as one of the fastest-growing thematic areas in their mapping of emerging circular-economy technologies, highlighting the need for further research into agricultural by-products with high material potential [9]. Although extensive research has been devoted to utilizing these by-products as low-cost adsorbents for environmental remediation, especially for organic pollutants and heavy metals present in aqueous media [4,10,11], these by-products have also proven to have potential for other applications, such as biofuel production (e.g., pellets or biochar) [12] or catalyst preparation for biodiesel production [13].

Grinding, as a common mechanical pretreatment method, has increasingly been applied to plum stones and other lignocellulosic biomass materials because of its ability to improve physicochemical properties by increasing surface area and porosity, two important factors in applications such as adsorption and biofuel production. It has been demonstrated that mechanochemical processes, such as extrusion and ball milling, can improve surface properties, expose functional groups, and break down native biomass structures without the need for chemical agents [14–18]. These changes improve the material's reactivity and the suitability for a range of energy and environmental applications [19,20]. Studies on cellulose and fruit-based residues have indicated that milling factors, such as speed, time, and ball-to-powder ratio, have an important influence on structural changes in biomass [21–23]. These results illustrate the importance of size reduction in enhancing environmental remediation performance and bioenergy conversion processes [24].

In addition, numerous studies have reported the use of various plant residues for the removal of metal ions and organic pollutants from wastewater, as well as their behavior during thermal degradation. For example, the use of lignocellulosic peach shell waste for Cu(II) ion biosorption was confirmed in a study by Lopičić et al. [25]. Furthermore, as work by Šoštarić et al. [26] showed, alkaline modification of apricot shell biomass enhanced porosity and crystallinity while slightly reducing thermal stability, indicating its potential for improved fuel properties in energy recovery applications. Pap et al. [27] showed that biochar derived from fruit processing waste is a highly effective adsorbent for phenolic compounds and heavy metals in industrial wastewater.

Although numerous studies have examined the use of lignocellulosic agricultural waste for various environmental and industrial applications, most have focused on chemical or thermal modifications to increase material performance. However, there is a notable deficiency of research on how specific mechanical milling parameters affect the structural and functional properties of plum stone biomass. Therefore, the aims of this study were to optimize the milling process of waste plum stones using a laboratory-scale planetary ball mill and to evaluate how varying milling parameters (rotational speed, milling time, and ball-to-powder ratio) influenced the resulting physicochemical properties. The purpose was to evaluate the products' potential for further utilization in sustainable and added-value applications, such as heavy metal adsorption.

## 2. Materials and Methods

The raw material used in this study consisted of washed, dried, and crushed plum stones with a particle size below 0.3 mm, obtained from agroindustrial waste.

To determine the particle size distribution, surface morphology, and compositional properties of the initial (untreated) material, X-ray diffraction (XRD), Fourier-transform infrared (FTIR) spectroscopy, scanning electron microscopy (SEM), and particle size analysis were conducted. XRD analysis of the raw material was performed to determine the phase composition using a Proto AXRD Benchtop Powder X-ray Diffractometer (Proto Manufacturing Inc., LaSalle, ON, Canada) with a Cu tube operated at 30 kV and 20 mA over a 2θ range of 10–40°. FTIR spectra were recorded in transmission mode using a BOMEM

spectrometer (Hartmann & Braun, Quebec, QC, Canada) within a wavenumber range of 4000–400 $cm^{-1}$. SEM analysis was conducted using a JEOL JSM-7001F field emission scanning electron microscope (JEOL Ltd., Tokyo, Japan) operated at an accelerating voltage of 20 kV. Prior to SEM imaging, the sample was mounted on carbon adhesive tape and coated with a thin layer of gold (15 nm thick layer, density 19.32 $g/cm^3$) using a Polaron SC503 sputter coater (Fisons Instruments, Ipswich, UK) to improve surface conductivity. Particle size analysis was performed using the ImageJ software. The analysis involved image thresholding, automated particle detection, and measurement of the Feret diameter as a representative parameter. Mechanical milling of the plum stone material was carried out using a planetary ball mill (SFM-1, model QM-3SP2; MTI Corporation, Richmond, CA, USA) equipped with 500 mL alumina grinding jars and 10 mm diameter alumina balls. Milling was performed at rotational speeds of 250 to 500 rpm, using ball-to-powder mass ratios of 10:1 and 20:1, with durations ranging from 1 to 3 h, as outlined in Table 1. Each milled sample is denoted with a unique abbreviation (PS-M1 to PS-M12), while the untreated sample is denoted as PS-U.

**Table 1.** Sample name and milling parameters for the plum stone samples (U—untreated; M—milled).

| Sample Name | Milling Time (h) | Milling Speed (rpm) | Ball-to-Powder Ratio |
|---|---|---|---|
| PS-U | / | / | / |
| PS-M1 | 1 | 250 | 10:1 |
| PS-M2 | 2 | 250 | 10:1 |
| PS-M3 | 3 | 250 | 10:1 |
| PS-M4 | 1 | 250 | 20:1 |
| PS-M5 | 2 | 250 | 20:1 |
| PS-M6 | 3 | 250 | 20:1 |
| PS-M7 | 1 | 500 | 10:1 |
| PS-M8 | 2 | 500 | 10:1 |
| PS-M9 | 3 | 500 | 10:1 |
| PS-M10 | 1 | 500 | 20:1 |
| PS-M11 | 2 | 500 | 20:1 |
| PS-M12 | 3 | 500 | 20:1 |

Following the milling process, FTIR, SEM, and particle size analyses were repeated to assess the effects of the milling parameters on the physicochemical properties of the material.

Investigation of the adsorption of metal ions $Pb^{2+}$ and $Cu^{2+}$ on selected samples was carried out to determine the influence of grinding parameters on the performance of plum stones as an adsorbent. The investigation included the calculation of adsorption efficiency, determination of kinetic models and adsorption isotherms.

Adsorption experiments were conducted using aqueous metal salts solutions prepared from lead(II) nitrate ($Pb(NO_3)_2$ and copper(II) sulfate (Fisher Chemical, Waltham, MA, USA), both prepared at an initial concentration of 100 $mg/dm^3$. A liquid-to-solid ratio of 200 was maintained as 1.0 g of the adsorbent was suspended in 200 $cm^3$ of the solution. The suspensions were agitated on an orbital shaker (Memmert, Schwabach, Germany) at 40 °C and 120 rpm for 24 h. Aliquot portions (3 $cm^3$) were taken from the suspension at predetermined time intervals (0.5, 1, 2, 4, 6, and 24 h), filtered through a 0.45 μm membrane filter, and analyzed. Residual $Pb^{2+}$ and $Cu^{2+}$ concentration in the filtrate was determined using a Perkin Elmer AAS Analyst 300 atomic absorption spectrophotometer (PerkinElmer, Waltham, MA, USA). For each time interval, the adsorption capacity ($q_t$, mg/g) was

calculated according to Equation (1), while adsorption efficiency was determined from the measured ion concentration after 24 h using Equation (2):

$$q_t = \frac{(C_0 - C_t)}{m} \cdot V \quad (1)$$

$$E = \frac{C_0 - C_t}{C_0} \cdot 100\% \quad (2)$$

where $C_0$ is the initial concentration of metal ion in the solution (mg/dm$^3$), $C_t$ is the concentration in the solution after the adsorption (mg/dm$^3$), $m$ is the mass of the adsorbent (g), and $V$ is volume of the suspension (dm$^3$).

The adsorption kinetics of $Pb^{2+}$ and $Cu^{2+}$ ions on plum stones samples was investigated using nonlinear pseudo-first-order (PFO) and pseudo-second-order (PSO) kinetic models, mathematically expressed as Equations (3) and (4), respectively:

$$q_t = q_1 \cdot (1 - e^{-k_1 \cdot t}) \quad (3)$$

$$q_t = \frac{{q_2}^2 \cdot k_2 \cdot t}{1 + q_2 \cdot k_2 \cdot t} \quad (4)$$

where $q_t$ is the adsorption capacity (mg/g) at time t (h); $q_1$ and $q_2$ (mg/g) are the equilibrium adsorption capacities for PFO and PSO, respectively; and $k_1$ (1/h) and $k_2$ (g/mg/h) are the PFO and PSO rate constants, respectively. The Excel solver add-in and the Runge–Kutta method were used to solve the nonlinear kinetic models and determine the kinetics constants, as described and provided in a paper by Wang and Guo [28]. Correlation coefficient ($R^2$) was applied to evaluate the fitting results and to compare the kinetic models.

To describe the relationship between the adsorption capacity and the equilibrium concentration of metal ions, the Langmuir and Freundlich isotherm models (Equations (5) and (6), respectively) were applied:

$$q_e = \frac{q_{max} \cdot K_L \cdot C_e}{1 + K_L \cdot C_e} \quad (5)$$

$$q_e = K_F \cdot {C_e}^{1/n_F} \quad (6)$$

where $q_e$ (mg/g) is the amount of adsorbed metal per gram of sorbent at the equilibrium; $C_e$ (mg/dm$^3$) is the equilibrium concentration of the solution; $q_{max}$ (mg/g) is the maximum adsorption capacity of the sorbent; $K_L$ (dm$^3$/mg) is the Langmuir constant; $K_F$ ((mg/g)·(dm$^3$/mg)$^{1/n}$) is the equilibrium constant, indicative of adsorption capacity; and $n_F$ is the adsorption equilibrium constant.

Adsorption isotherm experiments were performed at a liquid-to-solid ratio of 200, with 1 g of the adsorbent suspended in 200 cm$^3$ of the solution. The initial concentration of metal ions ranged from 20 to 120 mg/dm$^3$. The suspensions were agitated on an orbital shaker (Memmert GmbH + Co. KG, Schwabach, Germany) at 40 °C and 120 rpm for 24 h, followed by vacuum filtration using medium-porosity filter paper. The resulting filtrates were analyzed to determine the residual concentrations of $Pb^{2+}$ and $Cu^{2+}$ ions in the solution using atomic absorption spectroscopy.

The specific energy consumption during milling was estimated based on equipment specifications and operational conditions. The energy input was calculated using the Equation (7):

$$E\left(\frac{kWh}{kg}\right) = \frac{P \cdot t}{m} \quad (7)$$

where $p$ is the power of the milling device (0.75 kW), $t$ is the milling time (h), and $m$ is the mass of the processed plum stone sample (kg).

Depending on the sample, 10 g or 20 g of material was used, with milling durations ranging from 1 to 3 h. This setup enabled the estimation and comparison of specific energy input across various milling conditions.

The FTIR spectra of the milled samples were recorded in the range of 400–4000 $cm^{-1}$, but for detailed analysis, the region between 950 and 1850 $cm^{-1}$ was selected because of its relevance for oxygen-containing functional groups.

Deconvolution of overlapping peaks within this region was performed using a multipeak Gaussian fitting approach. The baseline was corrected, and the spectrum was smoothed before fitting. Each peak was fitted using a Gaussian function of the form expressed as Equation (8):

$$y = A \cdot e^{-\frac{(x-\mu)^2}{2\sigma^2}} \quad (8)$$

where $A$ is the peak amplitude, $\mu$ is the center (wavenumber), and $\sigma$ is the standard deviation related to peak width.

From the fitted curves, semiquantitative parameters including peak positions, full width at half maximum (FWHM), and integrated peak areas were extracted. These parameters were used to evaluate the abundance and structural characteristics of functional groups present on the material surface.

Statistical analysis was performed using one-way ANOVA to evaluate significant differences between PM1, PM10, and PM12 values. The statistical processing was conducted using NCSS 2021 (Number Cruncher Statistical Systems, Kaysville, UT, USA; accessed on 2 August 2025).

## 3. Results and Discussion

### *3.1. Characterization of the Untreated Plum Stone Sample*

Prior to analyzing the effects of milling, the PS-U sample was characterized using XRD, FTIR, SEM, and elemental (CHNS) analysis, providing insight into its crystalline structure, functional group composition, particle morphology, and elemental composition.

#### 3.1.1. Elemental Analysis of PS-U Sample

The obtained CHNS results were compared with data from the literature to confirm the typical lignocellulosic nature and biochemical balance of plum stones (Table 2).

The plum stone sample showed a moisture content of 5.21%, pH of 6.06, and redox potential (Eh) of 49.4 mV. Elemental CHNS analysis revealed high carbon (64.47%) and hydrogen (7.64%) content and moderate nitrogen (2.40%) content, corresponding to an estimated crude protein level of approximately 15%. The ash content was 2.3%, indicating a relatively rich mineral presence. Structural carbohydrate analysis showed 12.9% cellulose, 30.1% hemicellulose, and 35.7% lignin, confirming the typical woody nature of the plum seed shell.

The nitrogen level of 2.4% fell within the typical range reported in the literature for plum kernels (1.0–2.5%), indicating a protein content of approximately 15%. This makes the seed potentially suitable for partial use in nutritional or feed applications while remaining well-balanced in its biochemical composition.

**Table 2.** Elemental analysis of waste plum stones.

| Parameter | Value | Method | Literature Range [8,10,13,27,29] | Comment |
|---|---|---|---|---|
| Moisture | 5.21% | ASTM D2867-04 [30] | 6–10% | Low moisture, good for storage |
| pH | 6.06 | pH meter | 5.5–6.5 | Slightly acidic environment |
| Carbon (C) | 64.47% | Vario EL III C, H, N, S/O Elemental Analyzer (Elementar, Germany) | 50–65% | High organic matter content |
| Nitrogen (N) | 2.40% | | 1.0–2.5% | Approx. 15% crude protein (N × 6.25), within the typical range |
| Hydrogen (H) | 7.64% | | 6–8% | Typical for plant biomass |
| Sulfur (S) | 0.04% | | 0.02–0.1% | Low sulfur content, nontoxic level |
| Ash | 2.3% | ASTM [31] D2866-94 | 1–3% | Slightly above average, typical mineral content |
| Lignin | 35.7% | Klason, Kürschner–Hoffer methods | 30–40% | Typical for lignocellulosic biomass |
| Cellulose | 12.9% | | 10–15% | Within reported values |
| Hemicellulose | 30.1% | | 20–35% | On the higher side |

#### 3.1.2. XRD Analysis of PS-U Sample

The X-ray diffraction pattern of the untreated plum stone sample (PS-U), shown in Figure 1, revealed a crystalline phase corresponding to cellulose Iβ, characterized by diffraction peaks at approximately 14°, 16°, 22°, and 34° (2θ).

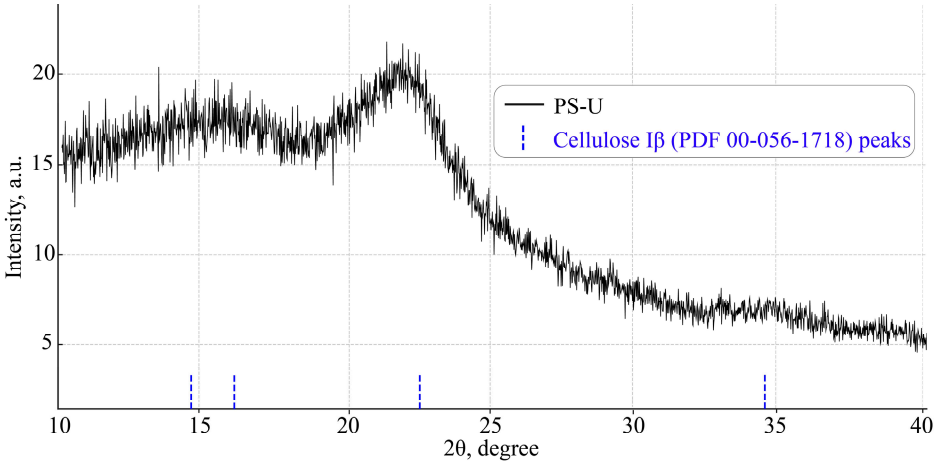



**Figure 1.** XRD pattern of the PS-U sample, with reference peak positions of cellulose Iβ (PDF 00-056-1718).

The observed peaks were broad and of low intensity, indicating a low degree of crystallinity, which is typical for biomass-derived materials [32]. In addition to cellulose Iβ as the dominant crystalline phase, a broad amorphous band between 2θ ≈ 18–30° was observed, corresponding to the presence of lignin and hemicellulose [32,33]. These findings confirmed the complex lignocellulosic nature of the plum stone structure.

### 3.1.3. FTIR Analysis of PS-U Sample

The FTIR spectrum of the PS-U sample (Figure 2) showed a broad absorption band at 3417 $cm^{-1}$, attributed to O–H stretching vibrations (alcohols and phenols), and a band at 2920 $cm^{-1}$, corresponding to C–H stretching in aliphatic chains. A weak peak at 1739 $cm^{-1}$ was associated with C=O stretching in esters or acids, while the band at 1617 $cm^{-1}$ was assigned to C=C stretching in aromatic rings (lignin). A strong band at 1104 $cm^{-1}$ indicated overlapping C–O–C and C–OH stretching, typical for glycosidic linkages and alcohols in cellulose and hemicellulose. These spectral features confirmed the lignocellulosic nature of the PS-U sample.

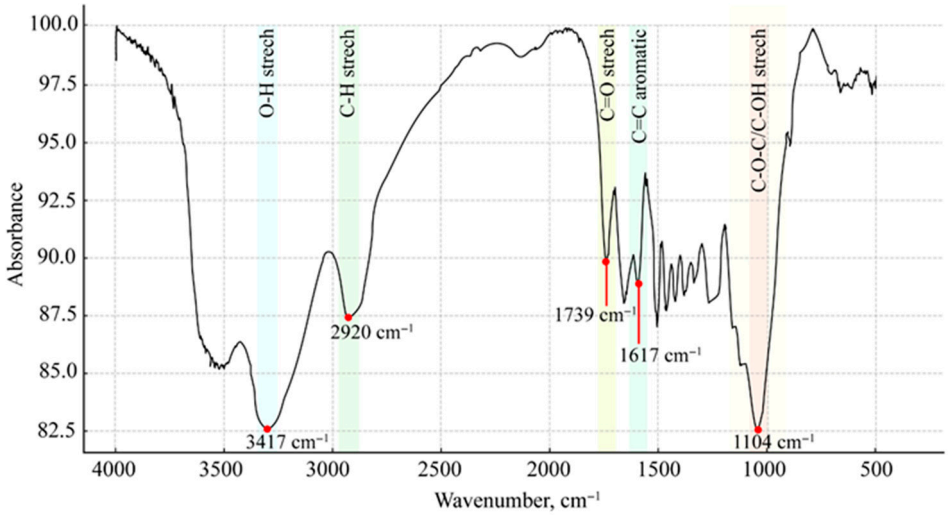



**Figure 2.** FTIR spectrum of the PS-U sample.

### 3.1.4. SEM Anaysis and Particle Size Distribution of PS-U Sample

Figure 3 presents the particle size distribution of the PS-U sample. The histogram (Figure 3) showed an asymmetric profile, with a dominant peak between 60 and 80 µm and a significant proportion of particles below 140 µm. Nevertheless, particles exceeding 300 µm were also present, indicating a broad distribution range.

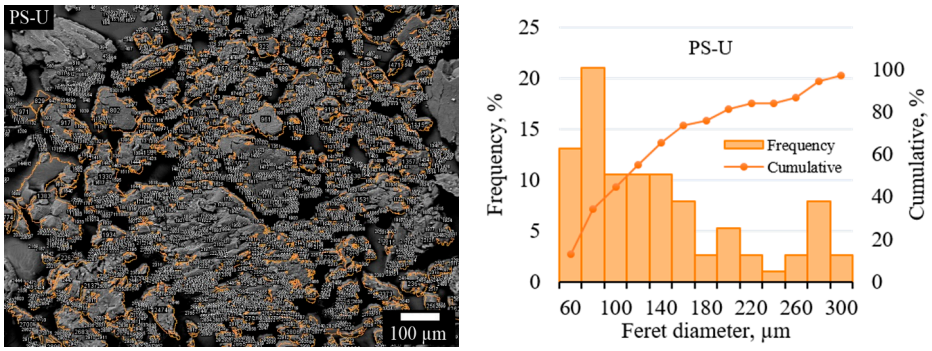



**Figure 3.** SEM photomicrograph of the PS-U with particle contours overlaid (ImageJ 1.54p analysis), and corresponding particle size distribution histogram with cumulative curve.

SEM analysis of the PS-U sample revealed a heterogeneous combination of large, irregularly shaped particles with lamellar, rough surfaces (Figure 4). Some particles retained fibrous structure and visible pores and cracks, confirming the unaltered lignocellulosic matrix, i.e., the absence of mechanical processing.

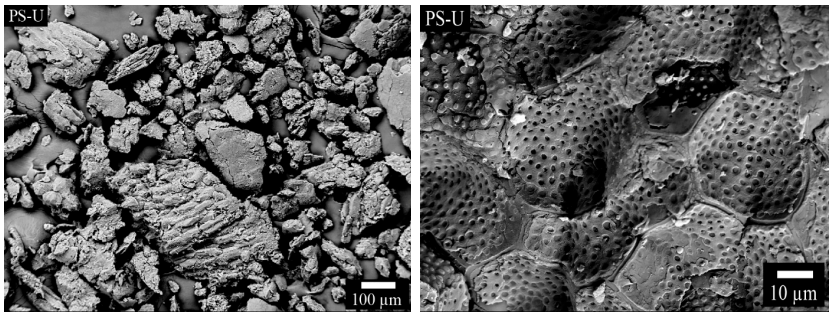



**Figure 4.** SEM photomicrographs of the PS-U sample at different magnifications.

### *3.2. Characterization of the Milled Plum Stone Samples*

The following results demonstrate how variations in mechanical treatment—rotational speed (250 and 500 rpm), milling duration (1–3 h), and ball-to-powder ratio (10:1 and 20:1)—affected the preservation or degradation of functional groups, particle size distribution, and surface morphology of the PS-M samples.

#### 3.2.1. FTIR Analysis of the Milled Plum Stone Samples

The FTIR spectra of the milled samples (Figure 5) showed all of the characteristic functional groups of the plum stone structure, including hydroxyl (O–H, ~3400 $cm^{-1}$), aliphatic (C–H, ~2920 $cm^{-1}$), carbonyl (C=O, ~1735 $cm^{-1}$), aromatic (C=C, ~1600 $cm^{-1}$), and ether (C–O–C, ~1050 $cm^{-1}$) vibrations.

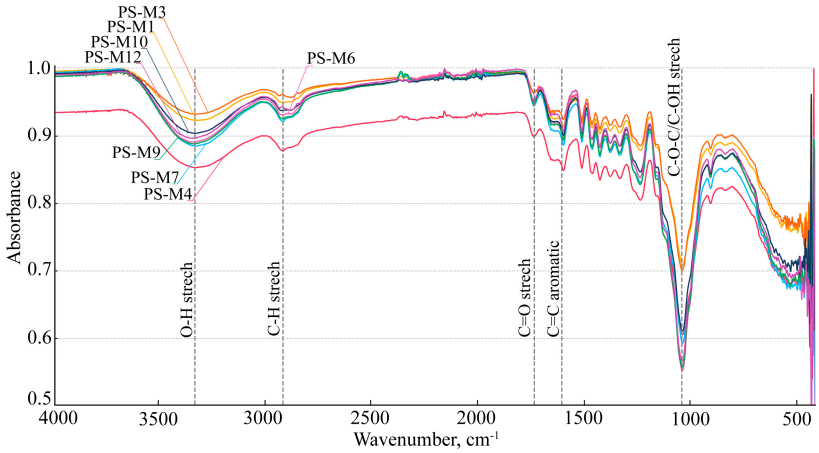



**Figure 5.** FTIR spectra of the milled samples.

Samples subjected to low-energy milling (e.g., PS-M1 and PS-M3; 250 rpm; 10:1 bpr) exhibited sharp and symmetric O–H (~3400 $cm^{-1}$) and C–H (~2920 $cm^{-1}$) absorption bands. With increased milling time up to 3 h, with constant rotational speed (250 rpm) and bpr (10:1), a broadening of these bands was observed, along with decreased intensity of the C–O–C band and increased presence of carbonyl and aromatic groups. This suggests partial chain scission and greater exposure of internal structures without complete degradation. In contrast, increasing the bpr to 20:1 at 250 rpm (PS-M4 and PS-M6) led to reduced absorbance, particularly for the C–O–C region, indicating degradation of polysaccharide linkages. The greatest reduction in functional groups was observed in the sample PS-M6 (3 h, 250 rpm, 20:1 bpr), confirming the cumulative effect of time and ball mass. Among the high-speed-milled samples (500 rpm), PS-M10 (1 h, 20:1 bpr) staood out for its prominent and well defined FTIR signals over all main functional group regions. In contrast, PS-M7, PS-M9, and PS-M12 exhibited broader or weakened signals, mostly in the O–H, C–H, and C–O–C regions. These findings suggest that short-duration, high-energy milling can

enhance surface activation without excessive functional group degradation. PS-M10 provided the most favorable balance between activation and preservation of surface chemistry, making it the most promising for adsorption applications.

In order to gain more detailed insights into the functional groups present on the surface of the milled samples, the FTIR spectra in the range of 950–1850 $cm^{-1}$ were subjected to Gaussian peak deconvolution. This semiquantitative approach allowed for the extraction of relevant spectral parameters such as peak positions, FWHM, and peak areas, which are associated with the abundance and structural environment of specific functional groups.

All analyzed samples (PS-M1 to PS-M12) exhibited multiple overlapping peaks in this region, corresponding primarily to stretching and bending vibrations of oxygen-containing groups such as C=O, C–O, and –OH, as well as aromatic skeletal vibrations.

When compared with other investigated samples (PS-M1 to PS-M12), PS-M10 exhibited the highest total relative share of oxygen-containing groups (C=O + C–O/C–O–C), exceeding 63%, whereas most other samples showed values in the 45–58% range. For example, PS-M4 had 24% C=O and 38% C–O/C–O–C, while PS-M7 contained 21% C=O and 35% C–O/C–O–C.

Overall, the deconvolution results confirmed the superior adsorption capacity of PS-M10, directly linking its performance to the high abundance of oxygen-containing and aromatic functional groups on the particle surface. The corresponding fitted peak parameters for PS-M10 are summarized in Table 3, and the deconvoluted FTIR spectrum is presented in Figure 6.

**Table 3.** Semiquantitative analysis of functional groups in PS-M10 based on FTIR peak deconvolution.

| Peak No. | Wavenumber Center ($cm^{-1}$) | FWHM ($cm^{-1}$) | Area (a.u. × $cm^{-1}$) | Relative Share (%) |
|---|---|---|---|---|
| 1 | 1695.76 | 30.33 | 69.081 | 1.8 |
| 2 | 1538.58 | 57.73 | 429.896 | 11.4 |
| 3 | 1480.19 | 28.15 | 211.376 | 5.6 |
| 4 | 1440.31 | 29.79 | 179.343 | 4.8 |
| 5 | 1393.60 | 44.25 | 337.625 | 9.0 |
| 6 | 1350.61 | 35.76 | 218.766 | 5.8 |
| 7 | 1293.29 | 71.92 | 800.572 | 21.3 |
| 8 | 1176.84 | 98.77 | 1508.935 | 40.2 |

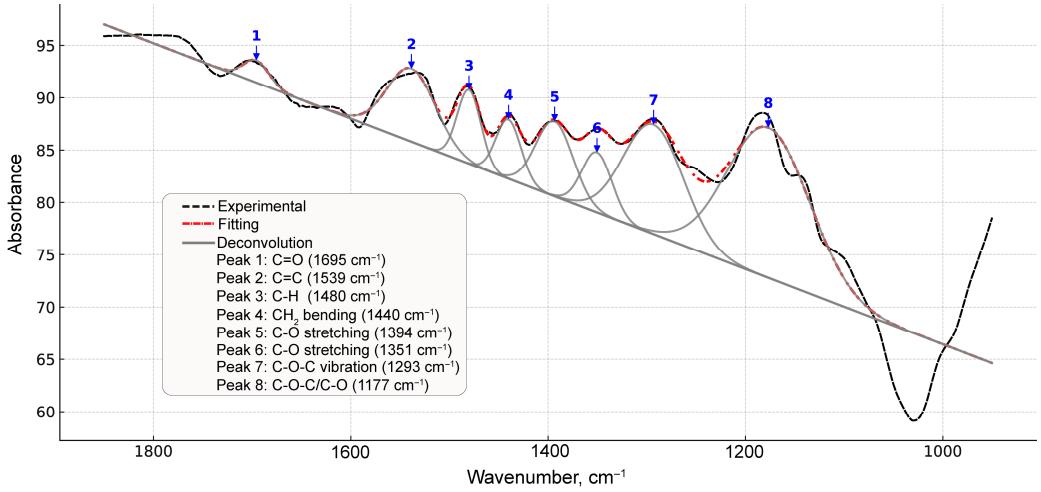



**Figure 6.** FTIR peak deconvolution of sample PS-M10 in the 950–1850 $cm^{-1}$ region.

3.2.2. SEM Anaysis and Particle Size Distribution of the PS-M Samples

SEM photomicrographs and corresponding Feret diameter histograms (Figure 7) showed clear morphological and particle size distribution differences among selected samples (PS-M10, PS-M12, and PS-M3). Sample PS-M10, milled at 500 rpm for 1 h with a 20:1 bpr, exhibited uniform morphology, with over 60% of particles below 10 µm, indicating effective mechanical treatment. In contrast, sample PS-M12 (same speed and ratio, 3 h) displayed coarser fractions, up to 90 µm, suggesting a broader distribution and possible reagglomeration due to prolonged milling. Sample PS-M3 (250 rpm, 3 h, and 10:1 bpr) showed the widest distribution, with very large particles (up to 150 µm), suggesting ineffective size reduction and homogenization despite prolonged milling time.

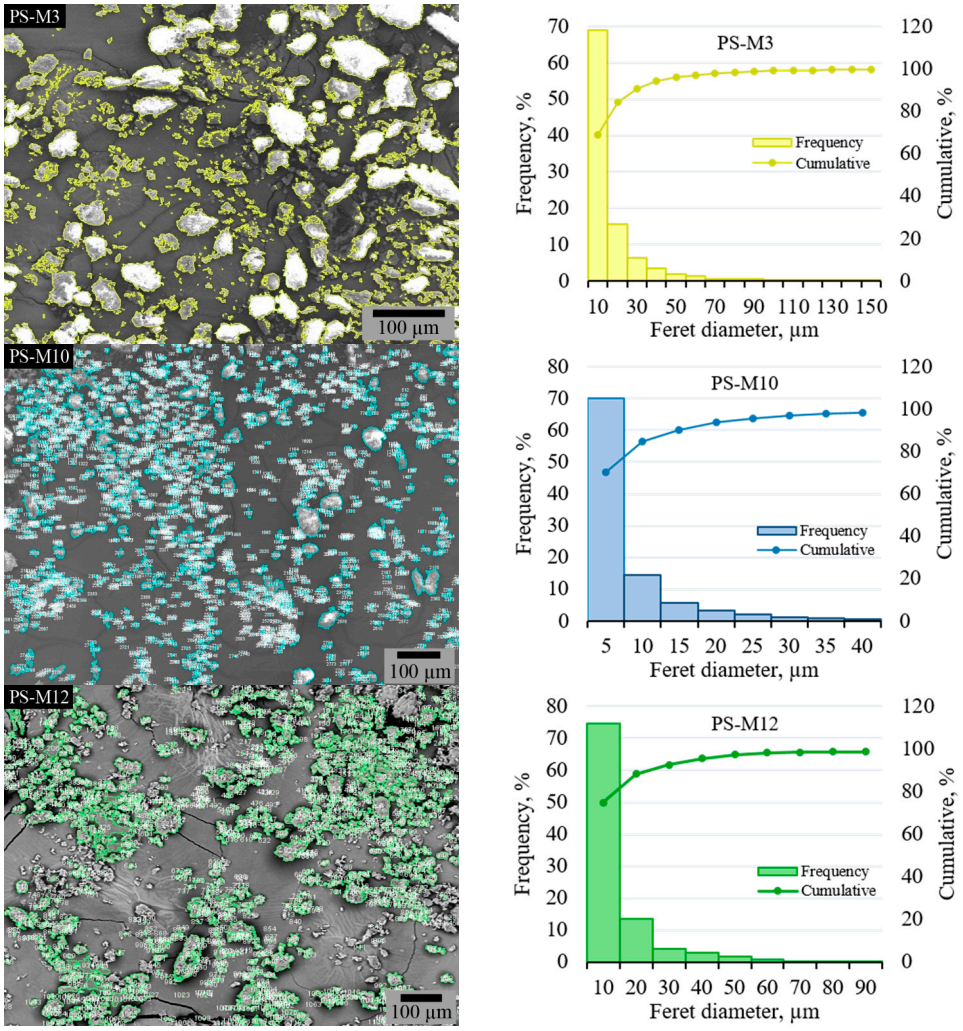



**Figure 7.** SEM photomicrographs of samples PS-M10, PS-M12, and PS-M3 with particle contours overlaid (ImageJ analysis) and corresponding particle size distribution histograms with cumulative curves.

Granulometric analysis (Figure 8) confirmed these trends through D10, D50, and D90 values. These characteristic Feret diameter values, corresponding to the proportion of fine, median, and coarse particle size, respectively, are crucial indicators of sample uniformity and overall quality. Samples milled at 250 rpm for shorter periods (PS-M1, PS-M4) had higher proportions of fine particles, indicating efficient reduction of samples without significant aggregation. Prolonged milling (PS-M6) or high-speed conditions (PS-M9, PS-M12) resulted in broader distributions and a presence of coarser fractions, indicating aggregation or overmilling. PS-M10 exhibited a balanced size profile, confirming

its best processing conditions. These variations in particle size distribution directly reflect the effectiveness of mechanical treatment and can significantly impact the surface reactivity and adsorption capacity of the resulting materials [16].

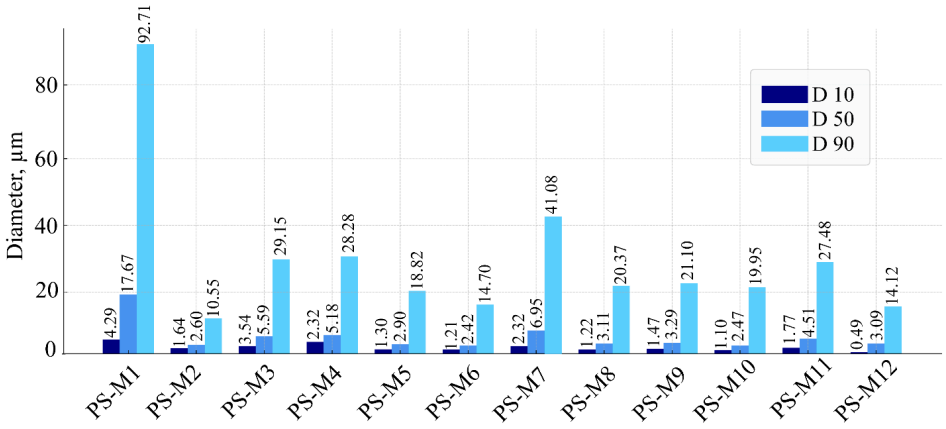



**Figure 8.** Comparison of Feret diameters (D10, D50, D90) for milled samples.

Further SEM analysis (Figure 9) showed morphological differences among the milled samples, supporting previous results and confirming the impact of milling parameters on the surface of particles.

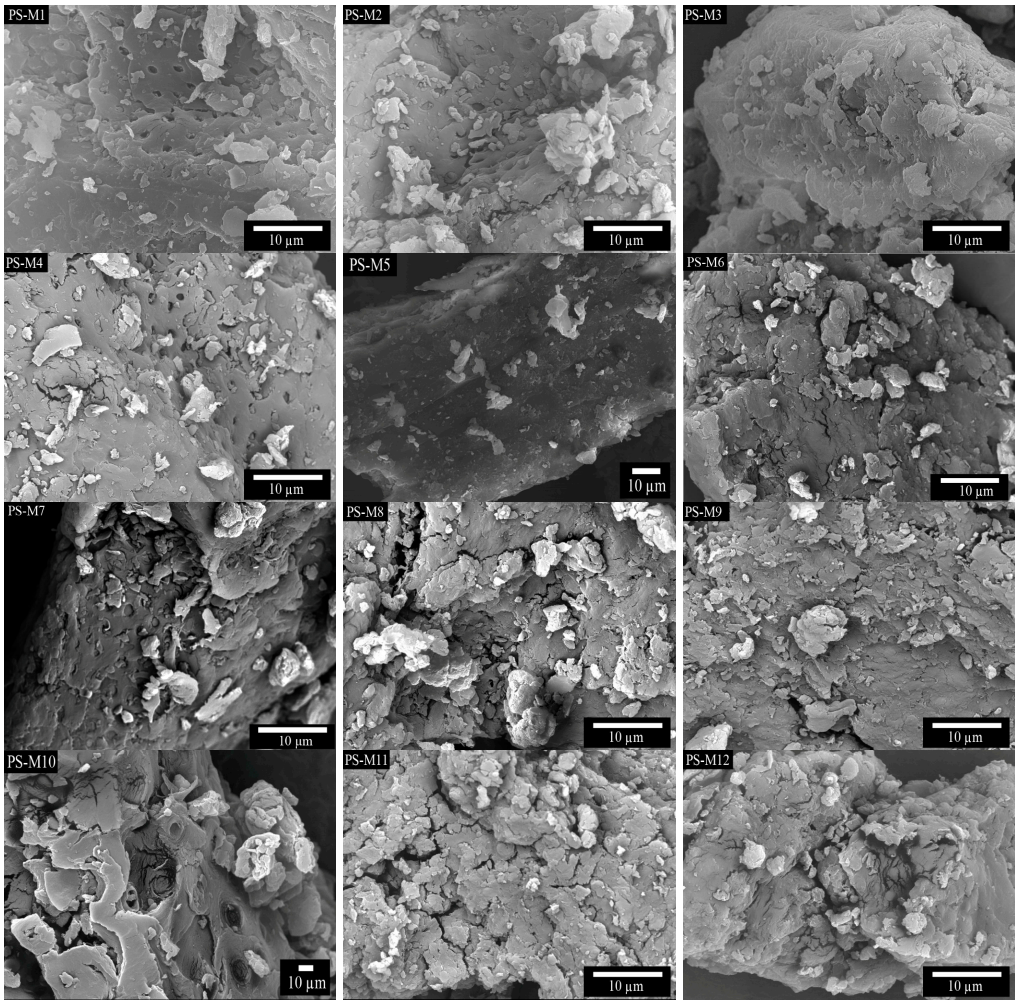



**Figure 9.** SEM photomicrographs of the PS-M samples.

Samples milled under low-energy conditions (PS-M1 to PS-M4) showed compact, smooth-surfaced particles with minimal roughness and visible aggregation, indicating limited size reduction and low surface activation. Medium-energy samples (PS-M5 to PS-M8) showed partial fragmentation, irregular shape, and surface texture development. The most obvious morphological changes were observed in samples PS-M10 and PS-M12, with porous, rough surfaces and high degrees of particle dispersion. Sample PS-M10 showed a porous structure and homogeneous distribution of fine particles, while PS-M12 exhibited finer fragments and irregular shapes. In the case of sample PS-M10, the short milling time limited structural degradation, while the high rotational speed (500 rpm) and increased ball-to-powder ratio (20:1) ensured sufficient surface activation.

### *3.3. Adsorption Performance of Selected Milled Plum Stone Samples*

#### 3.3.1. Adsorption Efficiency

To investigate the impact of various milling parameters on the application potential of treated plum stones, selected samples (PS-M1, PS-M10, and PS-M12) were tested for $Pb^{2+}$ and $Cu^{2+}$ ion removal from monocomponent aqueous solution. Samples of plum stones were obtained by milling them under various conditions, leading to different particle size distributions, FTIR spectra, and microstructures as analyzed by SEM. These variations resulted in differing adsorption efficiencies for $Pb^{2+}$ and $Cu^{2+}$ ions, as illustrated in Figure 10. The PS-M10 sample was the most effective in removing $Pb^{2+}$ (96.81%) and $Cu^{2+}$ ions (51.62%), followed by PS-M12, the adsorption efficiencies of which were 83.36% for $Pb^{2+}$ ions and 48.74% for $Cu^{2+}$ ions. The lowest efficiencies were observed for the PS-M1 sample, with 76.31% for $Pb^{2+}$ and 42.25% for $Cu^{2+}$ ions. These results are comparable to or exceed those found in the literature regarding the use of raw biowaste as an adsorbent. Bozecka et al. [34,35] studied the sorption of $Pb^{2+}$ ions from aqueous solutions using selected natural wastes. They achieved over 90% adsorption efficiency with sunflower hulls, approximately 80% with walnut shells, and around 75% with plum stones. In a study conducted by Gala and Sanak-Rydlewska [36], the depletion of $Pb^{2+}$ ions in solution ranged from 62.9% to 83.7% when using walnut shells as an adsorbent and from 47.2% to 81.3% for plum stones. Additionally, Marković et al. [37] reported about 85% adsorption efficiency with walnut waste biomass. Odobašić et al. explored the use of modified and unmodified plum stones as biosorbents for $Pb^{2+}$ ions from aqueous solutions, achieving around 30% removal efficiency with unmodified plum pits and 85% with modified plum pits after 60 min [12]. Research on the use of waste biomass for the removal of $Cu^{2+}$ ions from aqueous solutions has been significantly less extensive. Arroub and El Harfi [38] reported a removal of 69.5% $Cu^{2+}$ ions from liquid effluents using raw date stones, while Al-Ghouti et al. demonstrated approximately 80% removal efficiency of $Cu^{2+}$ ions using raw date pits of various particle sizes [39].

The process of sorbing metal ions from aqueous solutions involves several mechanisms, including ion exchange, chelation, and complexation. The effectiveness of these processes depends on the quantity and availability of active sites on the sorbent material. In the case of biosorbents, these active sites are primarily functional oxygen groups, particularly hydroxyl groups. These groups can donate a pair of electrons from oxygen to metal ions in the solution, enabling the sorbent to effectively bind metals from the solution [34,37,39]. Apart from the O–H groups (hydroxyl), the carbonyl group C=O (carboxylic compounds, esters, ketones, aldehydes, etc.) and the amine or amide groups may also play an important role in the sorption of metal ions [34]. Plum stones, as natural lignocellulosic materials, consist of three main components, namely cellulose, hemicellulose, and lignin. While lignin is a complex polymerized aromatic substance, both cellulose and hemicellulose primarily contain oxygen functional groups, such as hydroxyl, ether, and carbonyl [39].

FTIR analysis of milled plum pit samples indicated that intensive milling conditions result in partial degradation of functional groups. Consequently, the PS-M1 sample, milled under milder conditions (1 h, 250 rpm, 10 bpr), should have exhibited the highest adsorption efficiency. However, this was not the case. The limited size reduction and low surface activation of the PS-M1 sample, as confirmed by SEM analysis, contributed to its inferior performance. The surface area and the number of active sites of the adsorbent increased with decreasing particle size. Size reduction of the large particles serves to open sealed channels in the adsorbent, making them available for adsorption. Effectiveness of sorption also depends on the number of micro-, meso-, and macropores in the structure [39]. On the other hand, intensive grinding conditions, such as those observed in the PS-M12 sample, can cause small sorbent particles to aggregate. This aggregation restricts the accessibility of the functional groups on the sorbent surface to metal ions from the solution, resulting in a reduction in adsorption effectiveness [34]. The sample PS-M10 achieved the highest removal efficiency (96.81%), confirming that a short, high-energy milling process (500 rpm, 1 h, 20:1 bpr) is best for obtaining an activated surface without structural degradation.

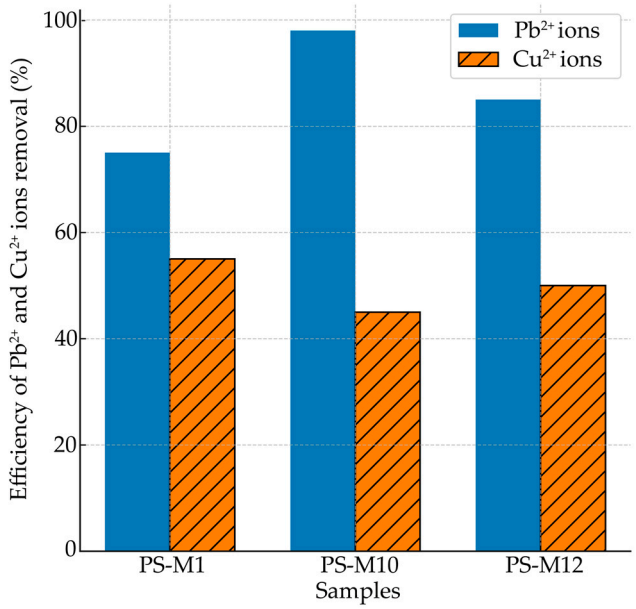



**Figure 10.** Adsorption efficiency of $Pb^{2+}$ and $Cu^{2+}$ ions onto selected milled plum stones.

To investigate the impact of various milling parameters on the application potential of treated plum stones, selected samples (PS-M1, PS-M10, and PS-M12) were tested for $Pb^{2+}$ ion removal from aqueous solution at a contact time of 60 min. As shown in Figure 10, PS-M10 achieved the highest removal efficiency (96.81%), confirming that a short, high-energy milling process (500 rpm, 1 h, 20:1 bpr) is best for obtaining a surface without structural degradation.

### 3.3.2. Adsorption Isotherms

Sorption isotherms are crucial for optimizing the adsorption processes because they describe the ratio between the mass of adsorbate and the mass of sorbent as a function of their concentration in solution, as well as the nature of the interaction between the adsorbate and the sorbent [37]. In this study of the sorption of $Pb^{2+}$ and $Cu^{2+}$ ions on selected samples of milled plum stones, two well-known isotherm models were utilized: Langmuir and Freundlich. The results of applying the nonlinear forms of these isotherms, using initial ion concentrations ranging from 20 to 120 mg/dm$^3$, are presented in Figure 11.

Additionally, the values of the coefficients from the isotherm equations and the correlation coefficient ($R^2$), are displayed in Table 4.

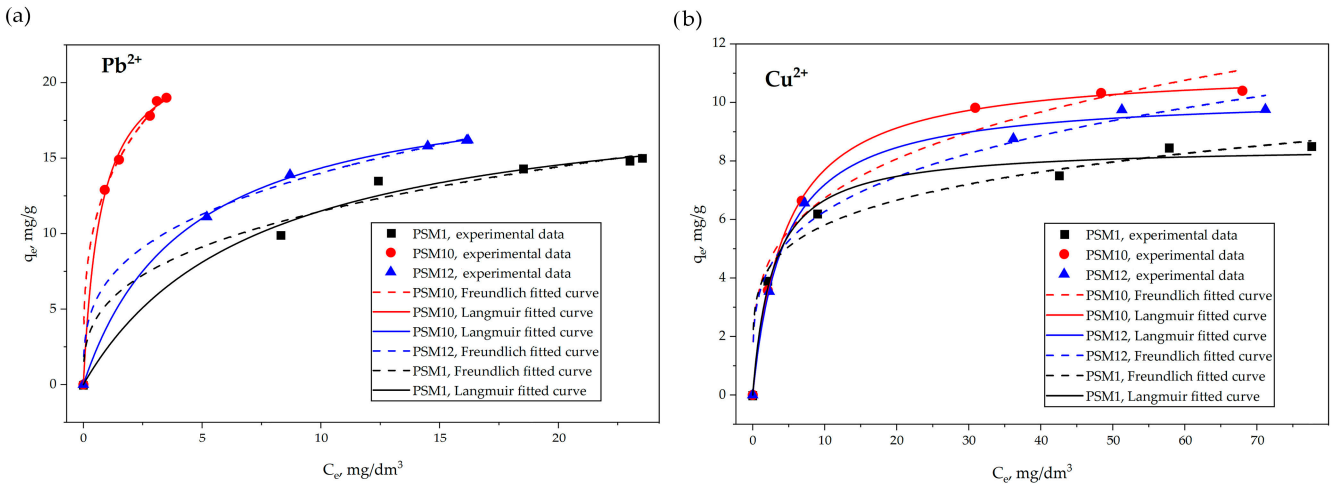



**Figure 11.** Langmuir and Freundlich adsorption isotherms for (**a**) $Pb^{2+}$ and (**b**) $Cu^{2+}$.

**Table 4.** Fitting parameters of Langmuir and Freundlich isotherm models.

| | | Langmuir Isotherm | | | Freundlich Isotherm | | |
|---|---|---|---|---|---|---|---|
| | | $q_{max}$ | $K_L$ | $R^2$ | $K_F$ | $1/n_F$ | $R^2$ |
| $Pb^{2+}$ | PS-M1 | 19.792 | 0.138 | 0.9909 | 5.349 | 0.331 | 0.9645 |
| | PS-M10 | 22.849 | 0.361 | 0.9981 | 13.277 | 0.292 | 0.9951 |
| | PS-M12 | 20.566 | 0.230 | 0.9997 | 6.806 | 0.314 | 0.9812 |
| $Cu^{2+}$ | PS-M1 | 8.513 | 0.359 | 0.9899 | 3.696 | 0.196 | 0.9638 |
| | PS-M10 | 11.207 | 0.219 | 0.9998 | 3.682 | 0.261 | 0.9574 |
| | PS-M12 | 10.268 | 0.234 | 0.9962 | 3.527 | 0.250 | 0.9537 |

The Langmuir isotherm implies monolayer adsorption of the adsorbate on the surface, which consists of a finite number of identical sites of homogeneous adsorption energy [34,37]. In this model, the process is limited by the number of active sites, leading to the creation of a single layer of molecules on the adsorbent's surface [40]. The constant $K_L$ represents the adsorption energy, so a lower value of the constant indicates a higher affinity of the sorbent for metal ions, while the $q_{max}$ constant represents theoretical value of the maximum sorption capacity of the sorbent, i.e., the maximum number of cations needed to form a complete monolayer [34]. In general, a good sorbent should be characterized by a lower value of the constant $K_L$ and a high value of the constant $q_{max}$ [37]. In the case of $Pb^{2+}$ ion adsorption on plum stones, the highest sorption capacity was found for the PS-M10 sample, $q_{max}$ 22.85 mg/g; this was very similar to the value for $q_{max}$ of 21.2 mg/g published in works by Gala and Sanak-Rydlewska [36] and Bozecka et al. [34]. The higher value for the adsorption capacity in this work was probably due to the reduced particle size for the PS-M10 sample compared with the samples from the literature (>0.5 mm). The maximum adsorption capacity for $Cu^{2+}$ ions was also found for the PS-M10 sample, $q_{max}$ 11.21 mg/g; comparative results could not be found in the literature.

The Freundlich model describes adsorption on an energetically heterogeneous surface on which the sorbed molecules are interactive. The constants in the Freundlich isotherm also provide valuable information about the adsorption process. The value of $K_F$ indicates the relative adsorption capacity of the adsorbent, a parameter related to the binding capacity of the adsorbate, while the value of 1/n is an indicator of the strength of adsorption. If the

value of 1/n is less than one, the adsorption process is considered to be of high intensity [12]. In the $Pb^{2+}$ ion adsorption process, the sample PS-M10 exhibited the highest $K_F$ value of 13.28, while in the $Cu^{2+}$ adsorption process, the $K_F$ values were similar for all three tested samples. Values of 1/n for all three investigated samples and both ions fell into the 0–1 range, indicating favorable adsorption of $Cu^{2+}$ and $Pb^{2+}$ onto milled plum stones [40].

The results of fitting the experimental data with both adsorption isotherms gave good results with $R^2$ values over 0.95 for all sets of experiments. However, comparing the results for the correlation coefficient, it can be concluded that the adsorption of $Pb^{2+}$ and $Cu^{2+}$ ions on milled plum stones followed the Langmuir isotherm, being mainly predominated by a monolayer, homogeneous adsorption process. Similar results were reported by Wang et al., for Ginkgo biloba L. shell-based adsorbent for the removal of $Cu^{2+}$ and $Cd^{2+}$ from aqueous solution [41]; Markovic et al., for the removal of $Pb^{2+}$ ions from aqueous solutions on walnut waste biomass [37]; and Areco et al., for the adsorption of $Zn^{2+}$, $Cu^{2+}$, $Cd^{2+}$, and $Pb^{2+}$ with *Avena fatua* biomass [42].

#### 3.3.3. Adsorption Kinetics

The study of adsorption kinetics is crucial for designing and scaling adsorption systems. It offers insights into the rate at which pollutants are removed, the mechanisms involved in the adsorption process, and the effectiveness of the adsorbent used. Among the various kinetic models proposed, the pseudo-first-order (PFO) and pseudo-second-order (PSO) are the most commonly employed for analyzing adsorption kinetics [43]. Experimental data obtained in adsorption tests of $Pb^{2+}$ and $Cu^{2+}$ ion were therefore fitted using the PFO and PSO kinetic models. The results of the parameters calculated from the nonlinear forms of the kinetic models are shown in Table 5 for their comparison.

**Table 5.** Adsorption kinetic constants for the adsorption of $Pb^{2+}$ and $Cu^{2+}$ on the PS-M1, PS-M10, and PS-M12 samples of milled plum stones.

| | | **PFO** | | | **PSO** | | |
|---|---|---|---|---|---|---|---|
| | | **$k_1$, 1/h** | **$q_1$, mg/g** | **$R^2$** | **$k_2$, g/mg/h** | **$q_2$, mg/g** | **$R^2$** |
| $Pb^{2+}$ | PS-M1 | 3.886 | 14.741 | 0.9967 | 0.822 | 15.063 | 0.9999 |
| | PS-M10 | 5.260 | 18.690 | 0.9993 | 1.221 | 18.961 | 0.9999 |
| | PS-M12 | 3.655 | 16.015 | 0.9985 | 0.616 | 16.466 | 0.9991 |
| $Cu^{2+}$ | PS-M1 | 2.481 | 7.614 | 0.9678 | 0.530 | 8.102 | 0.9914 |
| | PS-M10 | 2.604 | 8.896 | 0.9542 | 0.446 | 9.523 | 0.9962 |
| | PS-M12 | 2.429 | 8.254 | 0.9510 | 0.432 | 8.870 | 0.9919 |

The PFO and PSO models indicate that the rate of metal adsorption onto sorbent surfaces is proportional to the number of available sites. PFO kinetics are primarily influenced by physical adsorption processes, whereas PSO kinetics are governed by chemical interactions involving the sharing or exchange of electrons between the sorbent and the adsorbate [37]. The results presented in Table 5 showed correlation factors ($R^2$) greater than 0.95 for both the pseudo-first-order (PFO) and pseudo-second-order (PSO) models, indicating that both models accurately described the tested systems. The $R^2$ values for the PSO model, which were closer to 1 in all adsorption systems, suggest that the adsorption process follows second-order kinetics, highlighting chemical interaction as the dominant mechanism. This is in line with the discussion in the Section 3.3.1 on adsorption efficiency, which emphasizes that the functional oxygen groups on the surface of the biosorbent play the crucial role for the sorption of metal ions from aqueous solution, as they are oxygen electron donors to metal ions in their chemical bonding. Table 5 also shows that the ad-

sorption capacity values $q_1$ and $q_2$, calculated using the PFO and PSO models, respectively, had similar values for both ions and all three adsorbent samples. In addition, there was no significant deviation of these values from the $q_{max}$ obtained using the Langmuir adsorption isotherm. For instance, the adsorption capacity of $Pb^{2+}$ ions on the PS-M10 sample of milled plum stones, calculated with the Langmuir model, was 22.85 mg/g. In comparison, the PFO and PSO kinetic models predicted adsorption capacities of 18.69 mg/g and 18.96 mg/g, respectively, for the same process.

Gala and Sanak-Rydlewska [36] investigated untreated plum stones for $Pb^{2+}$ removal and reported efficiencies between 47.2% and 81.3% under conditions of ~5 g/L sorbent dose, with corresponding adsorption capacities of ~21.2 mg/g. Wiśniewska et al. [44] analyzed adsorption of KOH-activated plum-stone biochar and achieved adsorption capacities of up to ~178 mg/g and removal efficiencies above 90%, but the method required both chemical activation and high-temperature processing. Salikhanova et al. [11] showed high adsorption performance with steam-activated plum stones, but their method involved high-temperature activation at 800 °C.

Sample PS-M10 achieved a 96.8% $Pb^{2+}$ removal efficiency using only mechanical milling, with no chemical or thermal activation. Similar high $Pb^{2+}$ removal efficiencies have also been reported for composite materials, such as stone powder/chitosan/maghemite (SCM) beads, which have demonstrated effective adsorption performance in both batch and column studies [45]

Similar to mining waste recovery, where reuse offsets waste management costs and improves competitiveness [46,47], valorization of waste plum stones could reduce disposal costs for the plum-processing industry while generating added-value products. The uniform shape and strength of plum stones allow efficient milling, potentially lowering energy demand compared with other agricultural residues. If integrated on-site in processing facilities, this could minimize transportation and handling costs, improving economic feasibility. However, large-scale adoption will depend on consistent raw material supply, scalability, and a favorable balance between milling energy costs and the market value of the final product, which should be further evaluated under industrial conditions.

Furthermore, future studies could investigate the potential of using plum stones or other fruit stones as grinding media for processing low-strength minerals. Such evaluation should include wear resistance, grinding efficiency, and possible contamination of the processed material to determine their feasibility and safety in industrial mineral enrichment applications.

In addition to adsorption performance, energy consumption during the milling process is a critical factor in evaluating the sustainability of each treatment condition. Based on these findings, it can be concluded that the PS-M10 sample offered the most favorable compromise between adsorption efficiency and energy consumption. While it achieved the highest $Pb^{2+}$ and $Cu^{2+}$ removal among all tested samples, its estimated energy usage based on operational milling parameters remained moderate (~75 kWh/kg). In contrast, although PS-M12 also performed well, its threefold higher energy demand (~225 kWh/kg) reduced its sustainability. PS-M1, on the other hand, required the least energy (~37.5 kWh/kg) but showed substantially lower removal efficiency, making it more suitable for low-energy applications.

Besides its high $Pb^{2+}$ and $Cu^{2+}$ adsorption efficiency, the observed structural and surface characteristics of the PS-M10 sample (e.g., increased surface area, presence of oxygen-containing functional groups, and improved homogeneity) suggest its potential applicability for the adsorption of organic pollutants, integration into filtration systems, use as a precursor for activated carbon production, or incorporation into composite materials, further supporting its role in sustainable biomass valorization.

To assess the statistical significance of the structural changes induced by different milling parameters, a one-way ANOVA test was performed (Table 6).

**Table 6.** ANOVA results for particle sizes (Feret diameters) and FTIR band intensities of milled plum stone samples.

| Parameter | F Value [a,b] | *p* Value [b] |
|---|---|---|
| Feret diameters max | 15,850.49 | <0.00001 |
| Feret diameters min | 950.65 | <0.00001 |
| Feret diameters median | 554.19 | <0.00001 |
| Feret diameters average | 1744.55 | <0.00001 |
| FTIR 3335 $cm^{-1}$ | 17,730.37 | <0.00001 |
| FTIR 2881 $cm^{-1}$ | 20,613.47 | <0.00001 |
| FTIR 1733 $cm^{-1}$ | 145.86 | <0.00001 |
| FTIR 1558 $cm^{-1}$ | 460.83 | <0.00001 |
| FTIR 1030 $cm^{-1}$ | 2261.20 | <0.00001 |

[a] $F_{critical} = 5.14$; [b] $F_{stat} > F_{critical}$ and $p < 0.05$—arithmetic means are significantly different.

The analysis revealed significant differences in all monitored variables, including particle size descriptors (maximum, minimum, median, and average Feret diameters) and the intensities of key FTIR adsorption bands (3335, 2881, 1733, 1558, and 1030 $cm^{-1}$), with Fstat > Fcritical and $p < 0.00001$ in all cases. These results confirmed that variations in milling conditions substantially affected both the morphological and chemical characteristics of the plum stone material. Specifically, the significant shifts in FTIR peaks indicated modifications in the molecular structure and chemical bonding environment, while the pronounced differences in Feret diameters reflected changes in particle size distribution and surface morphology [48]. Taken together, the statistical evidence supports the conclusion that milling parameters are a critical factor in tailoring the physicochemical properties of ground biomass, with potential implications for its reactivity, processing behavior, and end-use applications.

## 4. Conclusions

This study investigated the effects of various milling parameters, including rotational speed (250 and 500 rpm), milling duration (1–3 h), and ball-to-powder ratio (10:1 and 20:1), on the morphology and adsorption properties of waste plum stones. The effects of these parameters were determined by using FTIR, SEM, and particle size distribution analyses. Accordingly, best conditions for surface activation while minimizing structural degradation were defined. The results demonstrated that mechanical processing significantly influences the morphology and surface chemistry of waste plum stone particles, directly affecting their potential for further applications such as heavy metal ion removal in wastewater treatment. Among the tested conditions, sample PS-M10 (500 rpm, 1 h, 20:1 bpr), showed the most favorable combination of fine particle distribution, preservation of key functional groups, and enhanced surface activation. These characteristics were confirmed by SEM, FTIR, and granulometric analysis, indicating that high-energy milling for a short time allows sufficient structural modification without excessive degradation. This balance was also reflected in the sample's superior adsorption performance, with over 96% $Pb^{2+}$ and 51.62% $Cu^{2+}$ removal efficiency, as confirmed by adsorption tests. These findings showed the potential of optimized mechanical treatment for converting agroindustrial waste into effective, sustainable materials for environmental applications. The findings presented

in this study are limited to the specific conditions and configuration of a laboratory-scale planetary ball mill (SFM-1, model QM-3SP2). As such, the optimization results, regarding rotational speed, milling time, and ball-to-powder ratio, may not be directly applicable to other types or scales of milling equipment. Additionally, the adsorption experiments focused on $Pb^{2+}$ ions under fixed conditions (initial concentration, temperature, contact time), which restricts the generalization of results to other heavy metals or environmental variables. Future studies should explore the effectiveness of the optimized PS-M10 sample for the removal of other heavy metals (e.g., $Cd^{2+}$, $Cr^{6+}$, $Zn^{2+}$) and organic pollutants (e.g., dyes, pesticides). In addition, future research should investigate other types of milling devices and a wider range of process parameters, with a focus on improving energy efficiency while maintaining the adsorption capacity of the material. It is also important to note that the optimization of milling parameters in this study was limited to specific laboratory conditions; therefore, future work should evaluate the scalability and industrial applicability of the proposed method.

**Author Contributions:** Conceptualization, N.G. and M.Š.; methodology, D.R.; software, N.G.; validation, S.J., I.J. and K.S.; formal analysis, I.J.; investigation, M.Š. and J.Đ.; resources, D.R.; data curation, N.G. and K.S.; writing—original draft preparation, N.G.; writing—review and editing, D.R., J.Đ. and N.G.; visualization, I.J. and N.G.; supervision, S.J. All authors have read and agreed to the published version of the manuscript.

**Funding:** This work was supported by the Ministry of Science, Technological Development, and Innovation of the Republic of Serbia (Contract No. 451-03-136/2025-03/200287 and 451-03-136/2025-03/200023).

**Data Availability Statement:** The original contributions presented in this study are included in the article. The data further supporting this study's findings are available from the first author, Nataša Gajić, upon reasonable request.

**Conflicts of Interest:** Authors Nataša Gajić, Dragana Radovanović, and Marija Štulović are employed by the Company Innovation Center of the Faculty of Technology and Metallurgy of the University of Belgrade. The remaining authors declare that the research was conducted in the absence of any commercial or financial relationships that could be construed as a potential conflict of interest.

## References

1. Food and Agriculture Organization of the United Nations. Crops and Livestock Products. Available online: https://www.fao.org/faostat/en/#data/QCL (accessed on 1 May 2025).
2. Milatović, D.; Zec, G.; Đurović, D.; Boškov, Đ. Production and processing of plum in Serbia. *Acta Agric. Serb.* **2020**, *25*, 59–63. [CrossRef]
3. Usmonova, Z.T.; Salikhanova, D.S. Change of functional groups and structure in the content of plum seed, carbonization, and activated carbon depending on temperature. *Univ. Tech. Sci.* **2024**, *7*, 17935. Available online: https://7universum.com/ru/tech/archive/item/17935 (accessed on 1 May 2025). [CrossRef]
4. Dołżyńska, M.; Obidziński, S.; Piekut, J.; Yildiz, G. The utilization of plum stones for pellet production and investigation of post-combustion flue gas emissions. *Energies* **2020**, *13*, 5107. [CrossRef]
5. Giri, D.D.; Jha, J.M.; Tiwari, A.K.; Srivastava, N. Java plum and amaltash seed biomass based bio-adsorbents for synthetic wastewater treatment. *Environ. Pollut.* **2021**, *280*, 116890. [CrossRef]
6. Katnić, Đ.; Marinović-Cincović, M.; Porobić, S.J.; Vujčić, I.; Šaponjić, A.; Sikirić, B.; Živojinović, D. Characterization and kinetics of thermal decomposition behavior of plum and fig pomace biomass. *J. Clean. Prod.* **2022**, *352*, 131637. [CrossRef]
7. Rubangakene, N.O.; Elkady, M.; Elwardany, A.; Fujii, M.; Sekiguchi, H.; Shokry, H. Novel nano-biosorbent materials from thermal catalytic degradation of green pea waste for cationic and anionic dye decolorization. *Biomass Convers. Biorefin.* **2023**, *13*, 14873–14888. [CrossRef]
8. Voća, N.; Bilandžija, N.; Jurišić, V.; Matin, A.; Krička, T.; Sedak, I. Proximate, Ultimate, and Energy Values Analysis of Plum Biomass By-products Case Study: Croatia's Potential. *J. Agric. Sci. Technol.* **2016**, *18*, 1655–1666.
9. Giordano, L.; Marras, F.; Mangiaracina, R.; Perego, A. Mapping Emerging Circular-Economy Technologies: A Topic Modeling Analysis. *PLoS ONE* **2024**, *19*, e0312709. [CrossRef]

10. Doczekalska, B.; Bartkowiak, M.; Kuśmierek, K.; Świątkowski, A. Activated carbons from plum stones as efficient adsorbents for the removal of phenol and bisphenol A from aqueous solutions. *Desalin. Water Treat.* **2023**, *306*, 51–62. [CrossRef]
11. Salikhanova, D.; Usmonova, Z.; Sobirjonova, S.; Ubaydullaeva, N.; Karabayeva, M. Obtainment of activated carbon by processing plum stones and using them in industrial wastewater purification. *E3S Web Conf.* **2024**, *486*, 01017. [CrossRef]
12. Odobašić, A.; Ahmetović, M.; Šestan, I.; Salihović, E.; Karić, A. Plum pits as natural sorbents for removal of lead ions. *Technol. Acta* **2021**, *14*, 33–37. [CrossRef]
13. Miladinović, M.; Pavlović, S.; Banković-Ilić, I.; Kostić, M.; Stamenković, O.; Veljković, V. Utilization of waste plum stones as a source of oil and catalyst for biodiesel production. *Hem. Ind.* **2023**, *77*, 39–52. [CrossRef]
14. Pérez Merchán, A.M.; Rodríguez Carballo, G.; Torres Olea, B.; García Sancho, C.; Maireles Torres, P.J.; Mérida Robles, J.; Moreno Tost, R. Recent advances in mechanochemical pretreatment of lignocellulosic biomass. *Energies* **2022**, *15*, 5948. [CrossRef]
15. Konan, D.; Koffi, E.; Ndao, A.; Peterson, E.C.; Rodrigue, D.; Adjallé, K. An overview of extrusion as a pretreatment method of lignocellulosic biomass. *Energies* **2022**, *15*, 3002. [CrossRef]
16. Di Domenico, G.; Cioccolo, E.; Bianchini, L.; Venanzi, R.; Colantoni, A.; Picchio, R.; Cozzolino, L.; Di Stefano, V. A Systematic Review of Mechanical Pretreatment Techniques of Wood Biomass for Bioenergy. *Energies* **2025**, *18*, 3294. [CrossRef]
17. Gallego-García, M.; Hernández-Serrano, A.; Salazar, A.; Urbano, B.; García-Sánchez, C. Recent advances on physical technologies for the pretreatment of lignocellulosic biomass: Milling, extrusion, ultrasound, and microwave methods. *Renew. Sustain. Energy Rev.* **2023**, *167*, 112720.
18. Sitotaw, Y.W.; Habtu, N.G.; Nunes, S.P.; Van Gerven, T. Mechanical pretreatment of lignocellulosic biomass: Milling as an initial step to enhance enzymatic hydrolysis. *iScience* **2022**, *25*, 104610. [CrossRef]
19. Wawrzaszek, B.; Charmas, B.; Jedynak, K. Impact of Mechanochemical Activation (MChA) on Characteristics and Dye Adsorption Behavior of Sawdust-Based Biocarbons. *Materials* **2024**, *17*, 4458. [CrossRef] [PubMed]
20. Li, Y.; Jin, Y.; Borrion, A.; Li, J.; Li, X. A critical review of pretreatment technologies to enhance anaerobic digestion and energy recovery. *Fuel* **2020**, *259*, 117494. [CrossRef]
21. Zheng, Y.; Fu, Z.; Li, D.; Wu, M. Effects of ball milling processes on the microstructure and rheological properties of microcrystalline cellulose as a sustainable polymer additive. *Materials* **2018**, *11*, 1057. [CrossRef]
22. Bian, R.; Li, L.; Ji, C.; Wang, Z. Effects of different mechanical treatments on structural changes of lignocellulosic waste biomass and subsequent Cu(II) removal kinetics. *Arab. J. Chem.* **2020**, *13*, 556–566. [CrossRef]
23. Kim, H.; Park, Y.; Lee, J. Engineering porosity and active sites in peach pit-derived carbon materials for high-performance sodium storage. *J. Energy Storage* **2025**, *65*, 116215. [CrossRef]
24. Mani, S.; Tabil, L.G.; Sokhansanj, S. Biomass feedstock pre-processing—Part 1: Pre-treatment. In *Biomass Conversion*; InTech: Rijeka, Croatia, 2011; pp. 1–18. [CrossRef]
25. Lopičić, Z.R.; Milojković, J.V.; Šoštarić, T.D.; Petrović, M.D.; Mihajlović, M.L.; Lačnjevac, Č.M.; Stojanović, M.D. Influence of pH value on Cu(II) biosorption by lignocellulose peach shell waste material. *Hem. Ind.* **2013**, *67*, 287–296. [CrossRef]
26. Šoštarić, T.; Petrović, M.; Stojanović, J.; Marković, M.; Avdalović, M.; Hosseini-Bandegharaei, A.-B.; Lopičić, Z. Structural changes of waste biomass induced by alkaline treatment. *Biomass Convers. Biorefin.* **2020**, *12*, 1051–1064. [CrossRef]
27. Pap, S.; Šoštarić, T.D.; Radonić, J.; Maletić, S.; Igić, S.; Turk Sekulić, M. Utilization of fruit processing industry waste as green activated carbon for the treatment of heavy metals and chlorophenols contaminated water. *J. Clean. Prod.* **2017**, *162*, 958–972. [CrossRef]
28. Wang, J.; Guo, X. Adsorption kinetic models: Physical meanings, applications, and solving methods. *J. Hazard. Mater.* **2020**, *390*, 122156. [CrossRef]
29. Núñez-Decap, M.; Wechsler-Pizarro, A.; Vidal-Vega, M. Mechanical, physical, thermal and morphological properties of polypropylene composite materials developed with particles of peach and cherry stones. *Sustain. Mater. Technol.* **2021**, *29*, e00300. [CrossRef]
30. *ASTM D2866-94*; Standard Test Method for Total Ash Content of Activated Carbon. ASTM International: West Conshohocken, PA, USA, 1999.
31. *ASTM D2867-04*; Standard Test Methods for Moisture Content of Activated Carbon. ASTM International: West Conshohocken, PA, USA, 2004.
32. French, A.D. Idealized powder diffraction patterns for cellulose polymorphs. *Cellulose* **2014**, *21*, 885–896. [CrossRef]
33. Poletto, M.; Ornaghi, H.L.; Zattera, A.J. Native Cellulose: Structure, Characterization and Thermal Properties. *Materials* **2014**, *7*, 6105–6119. [CrossRef] [PubMed]
34. Bozecka, A.; Bozecki, P.; Sanak-Rydlewska, S. Removal of Pb(II) and Cd(II) ions from aqueous solutions with selected organic wastes. *Physicochem. Probl. Miner. Process.* **2016**, *52*, 380–396. [CrossRef]
35. Bożęcka, A.; Bożęcki, P.; Sanak-Rydlewska, S. Study of chemical surface structure of natural sorbents used for removing of $Pb^{2+}$ ions from model aqueous solutions (Part II). *Arch. Min. Sci.* **2014**, *59*, 217–223. [CrossRef]
36. Gala, A.; Sanak-Rydlewska, S. A Comparison of $Pb^{2+}$ Sorption from Aqueous Solutions on Walnut Shells and Plum Stones. *Pol. J. Environ. Stud.* **2011**, *20*, 877–883.

37. Marković, D.; Bojić, D.; Bojić, A.; Nikolić, G. The biosorption potential of waste biomass young fruit walnuts for lead ions: Kinetic and equilibrium study. *Hem. Ind.* **2016**, *70*, 243–255. [CrossRef]
38. Arroub, H.H.; El Harfi, A. Preparation and characterization of carbons based on date stones: Application to the adsorption of $Zn^{2+}$ and $Cu^{2+}$ ions. *Appl. J. Environ. Eng. Sci.* **2019**, *5*, 131–143. [CrossRef]
39. Al-Ghouti, M.A.; Li, J.; Salamh, Y.; Al-Laqtah, N.; Walker, G.; Ahmad, M.N. Adsorption mechanisms of removing heavy metals and dyes from aqueous solution using date pits solid adsorbent. *J. Hazard. Mater.* **2010**, *176*, 510–520. [CrossRef]
40. Mikoda, B.; Klojzy-Karczmarczyk, B.; Mazurkiewicz, M.; Bąk, A. Air pollution control and flue gas desulfurization residues from Polish copper smelting facility as adsorbents of Pb (II) and Cu (II) from aqueous solutions. *Environ. Sci. Pollut. Res.* **2018**, *25*, 31520–31534. [CrossRef]
41. Wang, Z.; Shen, D.; Shen, F.; Wu, C.; Gu, S. *Ginkgo biloba* L. shells-based adsorbent for the removal of $Cu^{2+}$ and $Cd^{2+}$ from aqueous solution: Kinetics, isotherm, thermodynamics and mechanisms. *J. Mol. Liq.* **2017**, *241*, 603–611. [CrossRef]
42. Areco, M.M.; Saleh-Medina, L.; Trinelli, M.A.; Marco-Brown, J.L.; dos Santos Afonso, M. Adsorption of Cu(II), Zn(II), Cd(II) and Pb(II) by dead Avena fatua biomass and the effect of these metals on their growth. *Colloids Surf. B Biointerfaces* **2013**, *110*, 305–312. [CrossRef]
43. Zhao, J.; Boada, R.; Cibin, G.; Palet, C. Enhancement of selective adsorption of Cr species via modification of pine biomass. *Sci. Total Environ.* **2021**, *756*, 143816. [CrossRef] [PubMed]
44. Wiśniewska, M.; Marciniak, M.; Gęca, M.; Herda, K.; Pietrzak, R.; Nowicki, P. Activated Biocarbons Obtained from Plant Biomass as Adsorbents of Heavy Metal Ions. *Materials* **2022**, *15*, 5856. [CrossRef] [PubMed]
45. Song, G.; Oh, S. Adsorption of As and Pb by stone powder/chitosan/maghemite composite beads (SCM beads): Kinetics and column study. *Processes* **2023**, *11*, 581. [CrossRef]
46. Yıldız, T.D. Waste management costs (WMC) of mining companies in Turkey: Can waste recovery help meeting these costs? *Resour. Policy* **2020**, *68*, 101706. [CrossRef]
47. Kulczycka, J.; Góralczyk, M.; Włodarczyk, B. Cost of waste management versus competitiveness of mining: The example of non-ferrous metal industry. *Miner. Energy-Raw Mater. Rep.* **2003**, *18*, 10–15. [CrossRef]
48. Li, X.; Wang, Y.; Li, M.; Zhang, J.; Zhao, L. Effects of particle size distribution on the physicochemical, functional, and structural properties of alfalfa leaf powder. *Agriculture* **2024**, *14*, 634. [CrossRef]


**Disclaimer/Publisher's Note:** The statements, opinions and data contained in all publications are solely those of the individual author(s) and contributor(s) and not of MDPI and/or the editor(s). MDPI and/or the editor(s) disclaim responsibility for any injury to people or property resulting from any ideas, methods, instructions or products referred to in the content.